LAWRENCE
LIVERMORE
NATIONAL
LABORATORY

LLNL-JRNL-654350

Validation of attenuation models for ground motion applications in central and eastern North America

M. E. Pasyanos

May 13, 2014

Earthquake Spectra

Disclaimer

Validation of attenuation models for ground motion applications in central and eastern North America

Michael Pasyanos [a)]

We explore the use of recently-developed attenuation models in strong ground motion applications. The attenuation models are incorporated into standard 1-D ground motion prediction equations (GMPEs), effectively making them 2-D. This eliminates the need to create different sets of GMPEs for an increasing number of sub-regions. We test the model against a large dataset of over 10,000 recordings from 81 earthquakes in central and eastern North America. The use of attenuation models in the GMPEs improves our ability to fit observed strong ground motions in the region, sometimes significantly, and should be incorporated in future national hazard maps. The improvement is most significant at higher frequencies and longer distances which have a greater number of wave cycles. This has large implications for the rare, large magnitude (M>7.0) earthquakes, which produce potentially damaging ground motions over large areas, and which drive the seismic hazards in the region. Because the attenuation models can be created using weak ground motions, they could even be developed for regions of low seismicity where empirical recordings of strong ground motions are uncommon and do not span the full range of magnitudes and distances.

INTRODUCTION

The anelastic structure of the earth is a critical parameter in predicting ground motion amplitudes, and is one of the reasons, along with higher stress drops (e.g. Atkinson and Wald 2007), responsible for the well-documented variation in observed ground motions between tectonic regions like the western U.S. (WUS) and stable regions like the central and eastern U.S. (CEUS). One approach to deal with these variations has been to create appropriate ground motion prediction equations (GMPEs) for various regions, usually through the regression of empirical recordings of strong ground motions. The segment of the

[a)] Lawrence Livermore National Laboratory, 7000 East Ave., L-046, Livermore, CA 94550

seismological community focused on seismic hazards, however, has been slow in incorporating attenuation variations directly into the GMPEs, which would simplify the equations and allow finer spatial variations not represented in the GMPEs to be included. Impediments to doing so have been the lack of appropriate and reliable attenuation models and the demonstrated value of their inclusion. Here, we report on a previously-developed attenuation model for North America, discuss how the model can be best incorporated in ground motion estimates, and demonstrate their success in improving amplitude predictions on a very large dataset of strong ground motion recordings.

Besides incorporating variable attenuation in the GMPEs, a complementary approach will be to include the attenuation model in broad-band ground motion simulation techniques that are being used in the SCEC Broadband Simulation Platform (REF). In particular, we are simultaneously pursuing the inclusion of Q in simulations performed using the hybrid approach of Graves and Pitarka (2010). Early results indicate that the effect of attenuation is more significant at longer distances and at higher frequencies. It is especially important in regions where there are rapid changes between tectonics regions, including offshore regions that transition between oceanic and continental crust, as well as areas with rapid changes in sedimentary structure such as the Mississippi Embayment or San Francisco Bay.

ATTENUATION MODEL AND STRONG GROUND MOTION DATASET

In previous work we used the amplitudes of regional phases to determine the lithospheric attenuation structure of North America (Pasyanos 2013), producing maps of Qp and Qs for the crust and upper mantle. As discussed in Pasyanos (2011) and demonstrated for North America in Pasyanos (2013), we found that the use of the model could reduce the misfit between observed and predicted ground motion parameters relative to the 1-D GMPEs.

The development of the attenuation model was presented in depth in a recent paper (Pasyanos 2013) and will only be briefly summarized here. In short, we measure the absolute amplitudes of Pn, Pg, Sn, and Lg phases for hundreds of events and thousands of paths in North America in frequency bands from 0.5-10 Hz. The amplitudes are then used in a multi-phase inversion in which we simultaneously solve for Qp and Qs in the crust and upper mantle, as well as corresponding source and site terms. Since we will mainly be focusing on S-waves propagating in the crust, we show the Lg path map and crustal Qs maps in **Figure 1**.

Path coverage is excellent across the continental United States due to the station density and the fact that we are not limiting ourselves only to strong motions (**Figure 1a**). Since the

2013 paper (Pasyanos, 2013), we have made several updates. We have included more paths in Canada, Mexico, Central America, and the Caribbean, hoping to improve our coverage in these regions. The coverage outside the U.S. is still poor relative to within. We have incorporated more offshore events in order to improve our coverage out into the Atlantic and Pacific Oceans. In the 1-2 Hz passband, we now have a total of 14,000 amplitudes for 5,000 unique paths, recalling that we may have multiple phases for each path. We have also modified our starting Q in the oceans to be consistent with the values found in covered regions.

An inversion of the observed vertical amplitudes is performed for Q on a 0.5°x0.5° scale. We find a significant difference between the attenuation structure east and west of the Rocky Mountains, with the CEUS having significantly higher Q (lower attenuation) than the WUS (**Figure 1b**). This variation is reflected in the use of different GMPEs for these regions. The model shows significant variations in Q not only between the CEUS and WUS, but also additional variations within these broad regions (**Figure 1b**). For instance, there are large variations in Q that are associated with tectonic regions, such as the Basin and Range and the Colorado Plateau. There is also a substantial change in Q between the Gulf Coast and the rest of the CEUS. These high Q features generally continue north into Canada, although there are suggestions of low Q in the Alberta and Williston Basins. The low Q features of the tectonic WUS continue south into Mexico. There are also significant differences in the crustal Q between oceanic and continental regions, which can greatly affect the ground motions from offshore events.

We will validate our GMPEs by using the NGA East strong motion database (last accessed 8/31/2013). This is a very large dataset of observed strong ground motions of 94 well-distributed events in central and eastern North America, as well as two events from outside North America, which range in magnitude from 2.2 to 7.1 (**Figure 2**). We have eliminated the events occurring outside of North America and could not use a number of events which had no recordings of vertical amplitudes in the right frequency range, leaving us with a total of 81 events for our validation tests.

METHOD

Our strategy is to generalize the 1-D (distant dependent) GMPEs in order to isolate the attenuation term and to replace the Q inherent in the equations with the appropriate Q along the source-receiver path from our attenuation model. Although the attenuation models were

derived using Fourier amplitudes, the Q values should be equally applicable to the spectral amplitudes within each frequency band.

The ideal method of estimating ground motions using the model is the fully 3-D method that was described in Pasyanos (2013). With this technique, we propagate the Lg and Sn phases independently in a 3-D crustal model with variable crustal thickness and 2-D variations of Q in the crust and the upper mantle. Unfortunately, this is difficult to capture simply in the GMPEs. As an easier to implement method, we modify one of the terms of the 1-D GMPEs, as described below, with one that depends on the crustal attenuation along the path. This preserves the basic structure of the 1-D GMPEs, while allowing variable path attenuation. We will be using the GMPEs of Atkinson and Boore (2006), referred to in the rest of the text as AB2006, but this technique should be equally valid with other GMPEs.

Assume that ground motion amplitude as a function of frequency f can be described as:

$$A(f) = Ao \exp(-\pi f R/Q \beta) \quad (1)$$

or in log-space as:

$$\log_{10}A(f) = \log_{10}A_o - (\log_{10}e \pi f R) / (Q \beta) \quad (2)$$

where R is the epicentral distance, β is the shear wave velocity, Q is the attenuation quality factor, and A_o are amplitudes excluding the attenuation term.

From the GMPEs (Equation 5 in AB2006):

$$\log PSA = c_1 + c_2 M + c_3 M^2 + (c_4 + c_5 M) f_1 + (c_6 + c_7 M) f_2 + (c_8 + c_9 M) f_0 + c_{10} R_{cd} + S \quad (3)$$

where PSA is peak spectral acceleration, M is moment magnitude, R_{cd} the closest distance to the fault, f_0-f_2 are modified distance terms, S a site term (0 for hard rock sites) and c_1-c_{10} are empirically determined regressed coefficients. Equation 3 is also relevant for other parameters (e.g. SA, PGV) with different values for the coefficients. At large distances, relative to the critical distances, terms like f_0 either approach zero or, like $f_1 \rightarrow \log R_1$ and $f_2 \rightarrow \log R_{cd}$, become small relative to R_{cd}. At these distances, the spectral accelerations can be approximated as:

$$\log SA \approx C + c_{10} R_{cd} \quad (4)$$

where C summarizes the contributions of all the other terms.

Combining Equations 2 and 4 and assuming that, at long distances, $R_{cd} \sim R$, we find that:

$$c_{10} \approx (-\log_{10}e \pi f) / (Q \beta) \quad (5)$$

and hence:

$$Q \approx (-\log_{10} e\, \pi\, f) / (c_{10}\, \beta) \quad (6)$$

Entering values from Table 6 in AB2006 and, assuming that the observed ground motions are dominated by the crustally propagating S-wave phases (Sg, Lg), and β = 3.7 km/s, we determine the default apparent attenuation model built into these ground motion relations for eastern North America. This is shown by the green triangles in **Figure 3**, where the frequency-dependent Q over a significant portion of the frequency band can be approximated by a power-law form of $Q(f) = 750\, f^{0.4}$.

In addition to plotting Q derived from the GMPEs of AB2006, we have included Q values determined from the attenuation model of the lithosphere for North America (Pasyanos 2013). We have created two regions representing the WUS and CEUS which are shown by the red and blue boxes on **Figure 1b**. We then calculated the log-mean and standard deviation and plotted them as blue and red circles with associated error bars on **Figure 3**. It appears that the average Q of our CEUS model is compatible with, but slightly lower than the Q model built into AB2006, although there is significant variation in the Q structure of the CEUS region that we would like to capture by inclusion of a lateral attenuation model. The offset is likely an effect of differences in the geometrical spreading between the GMPEs and the attenuation tomography. In comparison, the WUS region has substantially lower Q than the CEUS, as well as significant variations. By replacing the c_{10} term with a values derived from Q as in Equation 5, we can easily incorporate 2-D attenuation effects into GMPEs, such as AB2006 or Campbell and Bozorgnia (2008).

The one situation where the two predictions can diverge significantly is where the crustal Q (Qc) is very low, causing the Lg phase to be highly attenuated or blocked. This is illustrated by **Figure 4**. Where values of Qc are normal, the crustal Sg and Lg phases dominate. Where Q is low, the amplitude of the crustal phase is reduced so significantly that the mantle phase (Sn) has the maximum observed amplitudes. In order to correct for this effect, when the 2-D ground motions are less than 50% of the 1-D ground motions, then the higher 1-D ground motions are used instead. At this point, this breakpoint is somewhat arbitrary and needs to be investigated further.

Figure 5 shows an example of predicted ground motions for 1-D, 1-D GMPEs with 2-D crustal Q, and for a 3-D model with variable crustal thickness and 2-D Q in the crust and upper mantle, along with observed ground motions for the 13 October, 2010 M4.3 earthquake in Slaughterville, OK. Because the Transportable Array component of USArray was in the central U.S. at the time of the earthquake, the earthquake was very well recorded. In **Figure**

5a, it is easy to see that the observed ground motions are not azimuthally independent, but record higher ground motions to the northeast. This is also observed in the Community Internet Intensity Map (CIIM; Wald et al. 1999) for the event (**Figure 5b**). Where there is variable Q, we see that the predicted ground motions are contorted and higher values extend to the northeast direction, as well as to the northwest. Importantly, there is not much difference in the predicted ground motions between **Figure 5c** and **Figure 5d** indicating that our approximate method is working well.

VALIDATION TESTS

We test the use of the attenuation model in predicting ground motion parameters (e.g. pseudo-spectral accelerations) by substituting along-path crustal Q for the 1-D Q built into the GMPEs, and do this for a large series of earthquakes in North America (see **Figure 2**). In order to compensate for the differences due to geometrical spreading described above, we have increased Q values by 25%. We show a few examples, highlighting a few points, such as the variations in attenuation within the central and eastern United States and large differences in crustal attenuation between oceanic and continental crust.

We will be performing the validations at two frequencies: 1 Hz and 5 Hz. At low frequencies like 1 Hz, the source amplitudes are primarily sensitive to the moment, which specifies the low-frequency source level, and is usually a well-known parameter for the events in our study. The attenuation model is also well-determined at this frequency, with a high number of recorded amplitudes, many crossing paths, and high resolution. In contrast, at higher frequencies the attenuation model is determined using fewer total amplitude measurements and fewer crossing paths, resulting in lower resolution and poorer coverage in some regions. Also at higher frequencies like 5 Hz, the source amplitudes are related to a combination of the seismic moment and the stress drop, which control the corner frequency. The stress drop is usually a more poorly determined parameter than the seismic moment (e.g. Cotton et al. 2013). For validation purposes, we will be using the moment magnitudes specified in the NGA-East dataset and a stress drop of 140 bars (14 MPa) in the AB2006 GMPEs, along with reference site conditions. At higher frequencies (up to 30 Hz) of interest for some of the systems, components, and structures of nuclear power plants, the effect of kappa (Anderson and Hough, 1984), which is not considered here, becomes increasingly important and limits the maximum high-frequency ground motions.

The first example is the 20 November, 2010 Mw 4.2 event in Guy, AR (**Figure 6**). Like the Slaughterville event, it was also a well-instrumented event due to presence of USArray. The AB2006 model generally does a relatively good job predicting ground motions for events like this in the CEUS. Like the previous example, we tend to see higher ground motions to the northeast and the contours of the variable attenuation model extend in this direction to capture this feature. The ground motion contours become condensed when they encounter oceanic crust in the Atlantic and thick sedimentary basins along the Gulf Coast and into the Gulf of Mexico. When we compare the predicted SAs to observations, the RMS misfit (in log-amplitude) is reduced from 0.448 to 0.384. Given the large scatter in the data, this misfit reduction is significant.

The second example is the 10 September, 2006 M5.85 event in the Gulf of Mexico (**Figure 7**). This is a region in the CEUS where AB2006 performs poorly. This is due to the fact that the crustal structure in the Gulf Coast and in the Gulf of Mexico, which has a thin crust, thick sediments, and low crustal Q, is so much different than the rest of the central and eastern North America. The use of separate GMPEs for the Gulf Coast and other regions like the mid-continent, has been done in the past (e.g. EPRI 1993) and is currently being pursued by a number of researchers. Comparing the predicted ground motions, we can see that, in the 2-D Q model, the ground motions are reduced even before they reach land, highlighting the importance of 2-D models for offshore earthquakes.

Because the crustal phases propagate poorly in oceanic crust, it is hard to get amplitude measurements in the region (see Lg path maps in **Figure 1a**). As a result, the attenuation model in these regions is somewhat more sensitive to the starting values of Q assigned to these regions, as they do not change significantly in the inversion. Due to the low Q in the Gulf and along the Gulf Coast, amplitudes are significantly reduced at observing stations on the continent. By incorporating Q into the existing GMPEs, we see a very significant reduction in RMS misfit from 0.862 to 0.371 without the need for a separate set of GMPEs.

RESULTS

The comparison that was performed for the two events shown in the previous section was performed for an additional 79 events (for a total of 81 events) at two frequencies: 1 Hz and 5 Hz. In all cases, we have only used recordings at near regional distances, excluding any observations beyond 1000 km. In general, the use of attenuation models in GMPEs improves our ability to fit observed strong ground motions in the region, sometimes significantly.

We use two metrics in assessing the model fits. The first is the RMS residual between the log-amplitude predictions and data, and the second is simply the log-amplitude difference between the two. In comparison to RMS, the log-amplitude difference preserves the sign of the misfit which allows us to see if the amplitudes are overpredicted or underpredicted. **Figure 8** plots the RMS and absolute difference between 1-D and 2-D at 1 Hz and 5 Hz. On both sets of plots, events where the 2-D model performs better (lower RMS or absolute differences closer to zero) are plotted in green and events where the 1-D model performs better are plotted in red. Predicted amplitude changes due to variable Q is less of an effect at lower frequencies like 1 Hz which have fewer wave cycles relative to high frequency data. Using 2-D Q produces lower residuals (both RMS and absolute differences) than 1-D Q about 60% of the time at 1 Hz and about 65% of the time at 5 Hz (**Figure 9ab)**. We expect these percentages to increase as the lateral and depth resolution of the attenuation model improves.

Somewhat surprisingly, there does not appear to be a strong geographic pattern (**Figure 9cd**), although the reason for this might not be very obvious. A small event in a region will only test the model out to near regional distances, while a larger event in the same region will generally have more recordings at both near regional and far regional distances. In all cases, the result is subject to station distribution.

There is still a lot of scatter in the data, indicating that the observed variations may be due to factors other than attenuation, such as source effects (focal mechanism / radiation pattern, directivity, stress drop), non-attenuation path effects (geometrical spreading), and site effects (site amplification, focusing/defocusing). These effects obviously remain in the data, as we seek to lower the scatter due to attenuation.

SCENARIO EARTHQUAKES

Note that in **Figure 6c** and **Figure 7c** the differences between the amplitudes predicted by the 1-D and 2-D GMPEs are largest for the smallest ground motions, observed at long distance ranges. We see smaller differences for the largest amplitudes, which are close in and dominated by geometrical spreading and source effects, and are relatively unaffected by attenuation variations. Although the relative differences are large, the absolute differences are comparatively small. This might suggest that these differences will be unimportant for seismic hazard assessment. This conclusion, however, would be wrong, as the small absolute differences that we find for small events are actually large absolute differences for large

magnitude events – differences that are observed over very large areas. In order to illustrate this, we show the differences in the predicted ground motions for several important scenario earthquakes for the central and eastern United States: New Madrid, MO, Charleston, NC, and Cape Ann, MA. Ground motions for all events were calculating assuming a standard stress drop of 140 bars (14 MPa). Since they are points of interest, the scenario figures are plotted with the location of nuclear power plants, which are from NASA's Global Change Master Directory (GCMD) (http://gcmd.nasa.gov). Keep in mind that we will be showing spectral accelerations at 1 Hz and these are always lower than the peak ground accelerations.

The 1811-1812 New Madrid, MO earthquakes were probably the largest historical earthquakes in the U.S. east of the Rockies (**Figure 10**). They occurred at the northern edge of the Mississippi embayment in the New Madrid seismic zone. Although the magnitude of these events has been somewhat disputed (e.g. Hough et al. 2000), the USGS lists the magnitude of the Dec. 16, 1811, Jan. 23, 1812, and Feb. 7, 1812 events as 7.7, 7.5, and 7.7 respectively. For the purposes of our scenario earthquake, we use an Mw of 7.7. This earthquake is particularly important, not only because it is a larger event, but also has the possibility of affecting many states above the 0.1g acceleration level. Differences between the 1-D and 2-D models are not large, suggesting that the attenuation structure in this region is close to the average for the CEUS. In general, we find that the ground motions are higher using the 2-D attenuation model, as indicated by the shaded regions in **Figure 10c**. The reduced ground motions to the south and southeast are consistent with the isoseismal map of Stover and Coffman (1993) (http://earthquake.usgs.gov/earthquakes/states/events/images/1811-1812_iso.gif).

The 1886 M7.3 Charleston, SC earthquake was the largest event in the southern U.S. (**Figure 11**). This earthquake is particularly important due to its proximity to many nuclear power plants located in the region. Here, we generally find lower predicted ground motions, except at long distances. Compared to the isoseismal map from Stover and Coffman (1993) (http://earthquake.usgs.gov/earthquakes/states/events/images/1886_09_01_iso.gif), the contours of the 2-D maps are similarly elongated to the northwest, and truncated to the northeast and southwest.

The 1755 M5.9 earthquake in Cape Ann, MA was the largest historic earthquake in the U.S. portion of the Boston-Ottawa seismic zone (**Figure 12**). While this is a relatively small earthquake, a repeat of the event, perhaps at a larger magnitude level, would affect a number of population centers in the northeast (e.g. Boston, New York, Philadelphia, Washington,

D.C. corridor). For purposes of our scenario, we have selected a magnitude of Mw 6.9, which is still below the estimated M_{max} for eastern North America. We find interesting differences between the ground motions predicted by the 1-D and 2-D Q models. We predict stronger ground motions in the continental interior and weaker ground motions along the coast, due to attenuation differences between the coastal and interior provinces.

CONCLUSIONS

In many regions of the earth, the number of recordings of large earthquakes is limited and recorded ground motion values are widely scattered. These two factors often make the empirical regressions of strong ground motion parameters impractical and inaccurate. We use information from the amplitude recordings of more frequent weak ground motions to develop an attenuation model of the crust and upper mantle which can be used to improve estimates of strong ground motions. Using the method outlined in the paper, we have easily been able to incorporate the attenuation models into existing GMPEs. The ground motions predicted with the 2-D models are more in agreement with intensity maps from historical earthquakes or modern equivalents like the CIIM. The use of more accurate attenuation models in GMPEs improves our ability to fit observed strong ground motions, sometimes significantly, and should be incorporated in future national hazard maps. We would expect these improvements to continue as the accuracy and resolution of the attenuation models improve. Attenuation models can also be used in broadband ground motion simulations that are performed to generate ground motion prediction equations for the East Coast and other regions where there is limited observed data.

Future work includes 1) improving the attenuation model, 2) validating the technique in other regions, and 3) incorporating the attenuation in ground motion simulations.The model can be improved by increasing resolution and extending the frequency band beyond the current 0.5-10 Hz to a wider frequency band. The resolution of the model could be improved significantly in the United States through the use of US Array data, which was not used in the development of the Pasyanos (2013) North American model. The increased seismicity in the CEUS (e.g. Ellsworth 2013) should provide more recordings of regional ground motions. In turn, with enough coverage, we could then improve the depth resolution by separating the effect of attenuation in the sediments and the crystalline crust. The model can be extended to higher frequency either by making more amplitude measurements at these frequencies (requiring high sampling rate recordings of these events) or by extrapolating from the

covered passband to higher frequencies using a power law assumption. The model can be extended to frequencies lower than 0.5 Hz by modeling the surface wave attenuation, since they dominate the amplitudes at these frequencies.

We would like to validate the technique in other regions including in the western United States using the NGA-West dataset or in Eurasia where a similar attenuation model has been developed (Pasyanos et al. 2009). With demonstrated success in other regions, we may be able to move towards a single universal set of GMPEs which would be applicable world-wide when provided with appropriate source (e.g. stress), path (e.g. attenuation), and site (e.g. Vs30, kappa) parameters.

ACKNOWLEDGMENTS

We thank Arben Pitarka for his input and comments on the manuscript. We kindly thank Christine Goulet for the NGA East strong ground motion parameter dataset that she provided for this study. We thank Norm Abrahamson for his suggestion to include scenario earthquakes. This was prepared under the auspices of the U.S. Department of Energy by Lawrence Livermore National Laboratory under contract DE-AC52-07NA27344. This is LLNL contribution LLNL-JRNL-******.

REFERENCES

Anderson, J.G. and Hough, S.E., 1984. A model for the shape of the Fourier amplitude spectrum of acceleration at high frequencies, *Bull. Seism. Soc. Amer.,* **74**, 1969-1993.

Atkinson, G.M. and Boore, D.M., 2006. Earthquake ground-motion prediction equations for eastern North America, *Bull. Seism. Soc. Amer.,* **96**, 2181-2205, doi: 10.1785/0120050245.

Atkinson, G.M. and Wald, D.J., 2007. "Did you feel it?" intensity data: a surprisingly good measure of earthquake ground motion, *Seism. Res. Lett.,* **78**, 362-368.

Campbell, K.W. and Bozorgnia, Y., 2008. NGA ground motion model for the geometrical mean horizontal component of PGA, PGV, PGD and 5% damped linear elastic response spectra for periods ranging from 0.01 to 10 s, *Earthquake Spectra*, **24**, 139-172.

Cotton, F., Archuleta, R. and Causse, M., 2013. What is sigma of the stress drop? *Seism. Res. Lett.*, **84**, doi: 10.1785/0220120087.

Electric Power Research Institute (EPRI), 1993. Guidelines for determining design basis ground motions: Vol. 1: Method and guidelines for estimating earthquake ground motions in eastern North America, EPRI TR-102293-V1, Palo Alto, CA.

Ellsworth, W.L., 2013, Injection-induced earthquakes, *Science*, **341**, DOI: 10.1126/science.1225942.

Graves, R.W. and Pitarka, A., 2010. Broadband ground-motion simulation using a hybrid approach, *Bull. Seism. Soc. Amer.,* **100**, 2095-2123, doi: 10.1785/0120100057.

Hough, S.E., Armbruster, J.G., Seeber, L., and Hough, J.F., 2000. On the modified Mercalli intensities and magnitudes of the 1811-1812 New Madrid earthquakes, *J. Geophys. Res.,* **105**, 23,839-23,864, doi: 10.1029/2000JB900110.

Pasyanos, M.E., Walter, W.R., and Matzel, E.M., 2009. A simultaneous multi-phase approach to determine P-wave and S-wave attenuation of the crust and upper mantle, *Bull. Seism. Soc. Amer.,* **99**, 3314-3325, doi: 10.1785/0120090061.

Pasyanos, M.E., 2011. A case for the use of 3D attenuation models in ground-motion and seismic-hazard assessment, *Bull. Seism. Soc. Amer.,* **101**, 1965-1970, doi: 10.1785/0120110004.

Pasyanos, M.E., 2013. A lithospheric attenuation model of North America, *Bull. Seism. Soc. Amer.,* **103**, 3321-3333, doi:10.1785/0120130122.

Stover, C.W. and Coffman, J.L., 1993. Seismicity of the United States, 1568-1989 (revised), USGS Professional Paper 1527, 418 pp.

Wald, D.J., Quitoriano, V., Dengler, L.A., and Dewey, J.W., 1999. Utilization of the Internet for rapid community intensity maps, *Seism. Res. Lett.*, **70**, 680-697.

Figure Captions

Figure 1. a) Path map of study area showing path coverage of Lg phase in the 1–2 Hz passband. On all figures, open circles indicate events and yellow triangles indicate stations. b) Map of lateral variations in the attenuation parameter Q in North America for crustal Q_S in the 1–2 Hz passband. Q is plotted on a logarithmic scale.

Figure 2. Map showing earthquakes in the NGA-East strong motion database located in central and eastern North America. Green circles are earthquake locations scaled by event magnitude. Map inset shows several events in the Northwest Territories of Canada.

Figure 3. Attenuation parameter Q as a function of frequency as derived from the Atkinson and Boore (2006) model (green triangles) and ranges of Q from North America attenuation model (Pasyanos 2013) for the Central and Eastern United States (CEUS; blue circles) and for the Western United States (WUS; red circles), where the symbols represent the log-mean and corresponding bars the standard deviation.

Figure 4. Predicted spectral accelerations vs. distance for a number of crustal Q values. Green lines show the amplitudes of the Sg/Lg phases for various Q values, while the blue line shows Sn amplitudes. This line is plotted as dashed where it is non-geometric.

Figure 5. Ground motions for a M4.3 earthquake in Slaughterville, OK. a) 1 Hz spectral accelerations predicted from 1-D GMPEs shown by solid black contour lines. Observed spectral accelerations are indicated by colored triangles. b) 1 Hz spectral accelerations predicted from 1-D GMPEs with 2-D crustal Q shown by solid black lines. c) 1 Hz spectral accelerations predicted from a 3-D model with 2-D Q in the crust and upper mantle shown by solid black lines.

Figure 6. Ground motions for a M4.2 earthquake in Guy, AR. a) 1 Hz spectral accelerations predicted from 1-D GMPEs shown by solid black contour lines. Observed spectral accelerations are indicated by colored triangles. b) 1 Hz spectral accelerations predicted from 1-D GMPEs with 2-D crustal Q shown by solid black lines. c) Comparison of 1-D and 2-D predicted 1 Hz spectral accelerations to observed spectral accelerations.

Figure 7. Ground motions for a M5.85 earthquake in the Gulf of Mexico. a) 1 Hz spectral accelerations predicted from 1-D GMPEs shown by solid black contour lines. Observed spectral accelerations are indicated by colored triangles. b) 1 Hz spectral accelerations predicted from 1-D GMPEs with 2-D crustal Q shown by solid black lines. c) Comparison of 1-D and 2-D predicted 1 Hz spectral accelerations to observed spectral acceleratons.

Figure 8. Comparison of misfit between GMPEs and observed ground motions between 1-D and 2-D GMPEs. a) Plot of 1-D RMS (x-axis) vs. 2-D RMS (y-axis) for 1 Hz spectral accelerations. Green symbols indicate lower misfit for 2-D, while red symbols indicate lower misfit for 1-D. b) Plot of 1-D RMS (x-axis) vs. 2-D RMS (y-axis) for 5 Hz spectral accelerations. c) Plot of 1-D Difference (x-axis) vs. 2-D Difference (y-axis) for 1 Hz spectral accelerations. d) Plot of 1-D Difference (x-axis) vs. 2-D Difference (y-axis) for 5 Hz spectral accelerations.

Figure 9. a) Histograms of best model for RMS at 1 Hz and 5 Hz. b) Histograms of best model for absolute differences at 1 Hz and 5 Hz. c) Map showing locations of events along with indication of better model for 1 Hz RMS (left half of circle) and 5 Hz RMS (right half of circle). d) Map showing location of events along with indication of better model for 1 Hz difference (left half of circle) and 5 Hz difference (right half of circle). In all figures, green indicates 2-D model has lower misfit than the 1-D model, while red indicates the 2-D model has a higher misfit than the 1-D model.

Figure 10. Predicted ground motions for a M7.7 New Madrid, MO earthquake. a) 1-D predicted 1 Hz spectral accelerations shown by solid black contour lines. b) 2-D predicted 1 Hz spectral accelerations shown by solid black contour lines. c) Difference between 1-D and 2-D predicted spectral accelerations show by solid black contour lines. Green symbols indicate the location of nuclear power plants.

Figure 11. Predicted ground motions for a M7.3 Charleston, SC earthquake. a) 1-D predicted 1 Hz spectral accelerations shown by solid black contour lines. b) 2-D predicted 1 Hz spectral accelerations shown by solid black contour lines. c) Difference between 1-D and 2-D predicted spectral accelerations show by solid black contour lines. Green symbols indicate the location of nuclear power plants.

Figure 12. Predicted ground motions for a M6.9 Cape Ann, MA earthquake. a) 1-D predicted 1 Hz spectral accelerations shown by solid black contour lines. b) 2-D predicted 1 Hz spectral accelerations shown by solid black contour lines. c) Difference between 1-D and 2-D predicted spectral accelerations show by solid black contour lines. Green symbols indicate the location of nuclear power plants.

Figure 1

a)

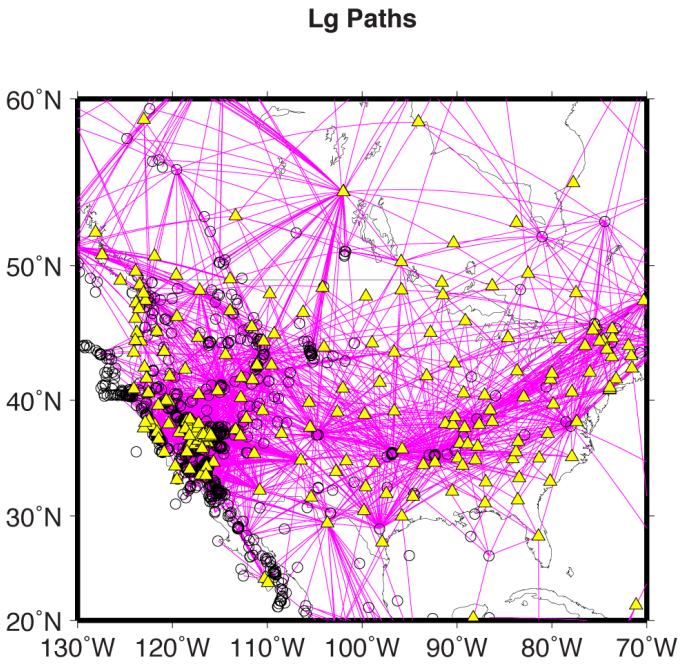
Lg Paths
60˚N
50˚N
40˚N
30˚N
20˚N
130˚W
120˚W
110˚W
100˚W
90˚W
80˚W
70˚W

b)

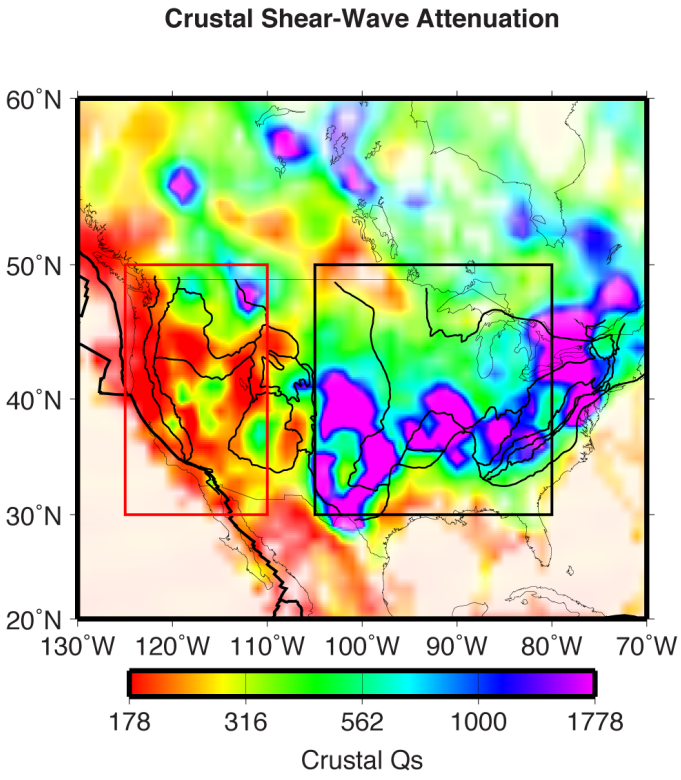
Crustal Shear-Wave Attenuation
60˚N
50˚N
40˚N
30˚N
20˚N
130˚W
120˚W
110˚W
100˚W
90˚W
80˚W
70˚W
178
316
562
1000
1778
Crustal Qs

Figure 2

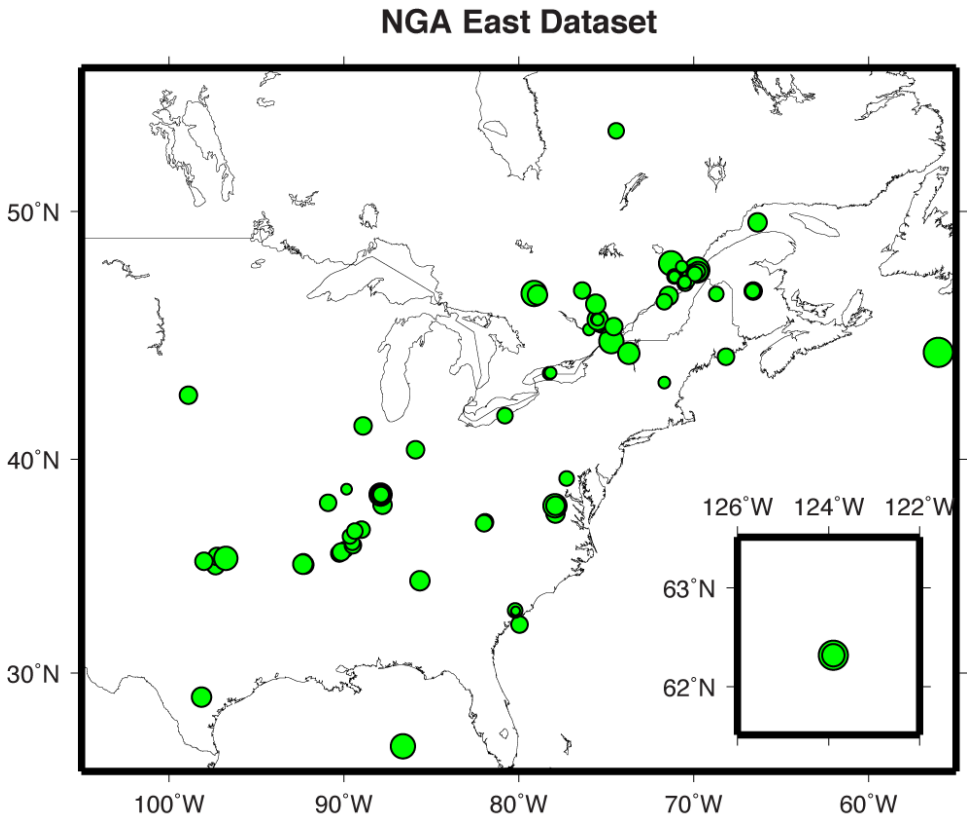
NGA East Dataset
50˚N
40˚N
30˚N
100˚W
90˚W
80˚W
70˚W
60˚W
126˚W
124˚W
122˚W
63˚N
62˚N

Figure 3

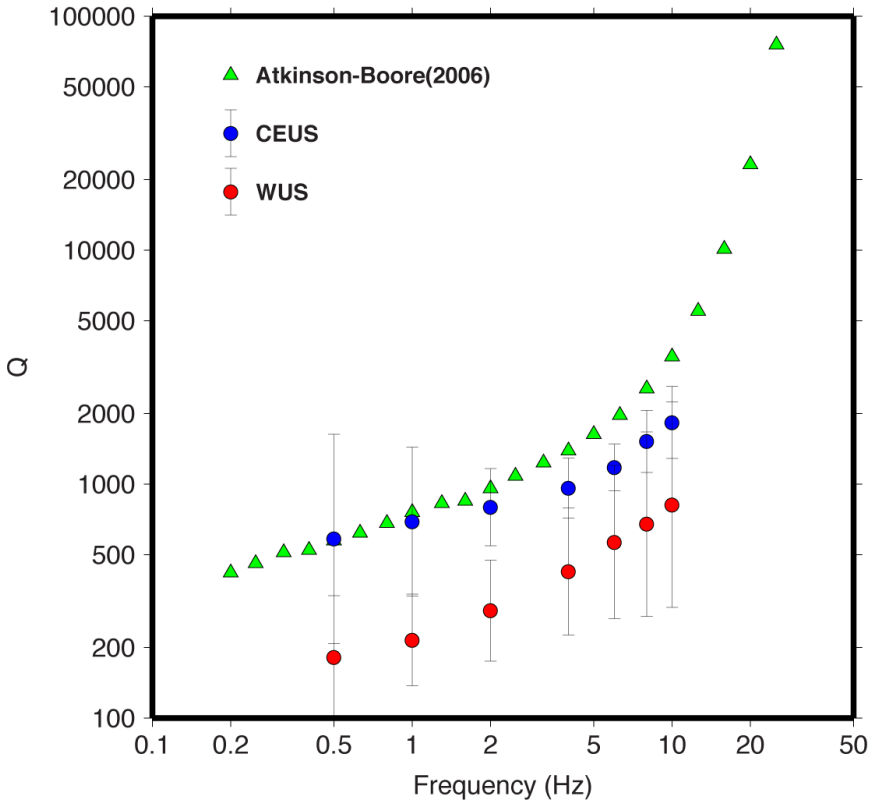
Atkinson-Boore(2006)
CEUS
WUS
Q
Frequency (Hz)
100000
50000
20000
10000
5000
2000
1000
500
200
100
0.1
0.2
0.5
1
2
5
10
20
50

Figure 4

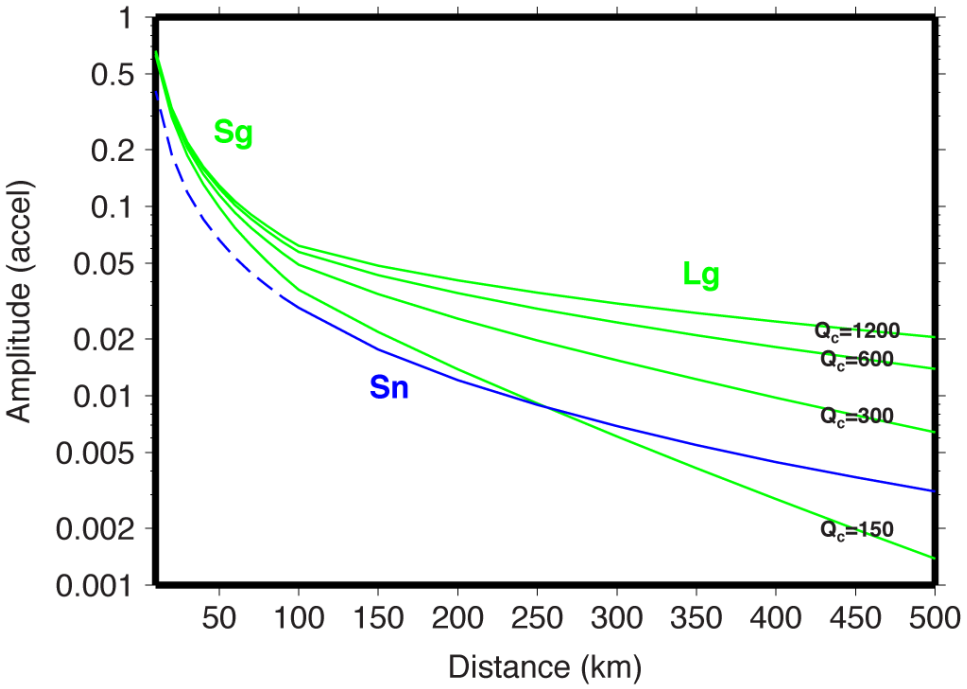
Amplitude (accel)
1
0.5
0.2
0.1
0.05
0.02
0.01
0.005
0.002
0.001
50
100
150
200
250
300
350
400
450
500
Distance (km)
Sg
Lg
Sn
Qc=1200
Qc=600
Qc=300
Qc=150

Figure 5

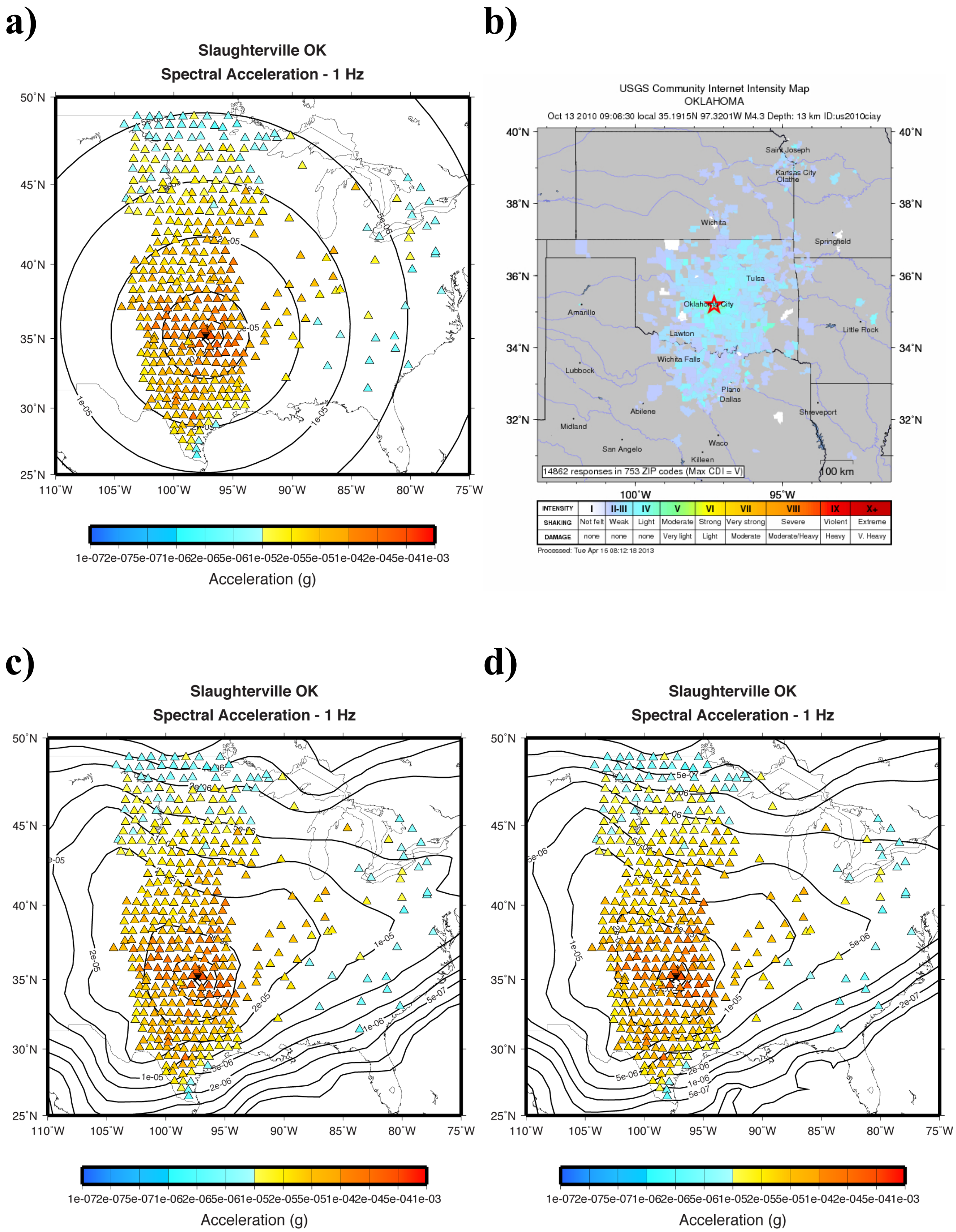

a)
Slaughterville OK
Spectral Acceleration - 1 Hz
50˚N
45˚N
40˚N
35˚N
30˚N
25˚N
110˚W
105˚W
100˚W
95˚W
90˚W
85˚W
80˚W
75˚W
1e-072e-075e-071e-062e-065e-061e-052e-055e-051e-042e-045e-041e-03
Acceleration (g)
b)
USGS Community Internet Intensity Map
OKLAHOMA
Oct 13 2010 09:06:30 local 35.1915N 97.3201W M4.3 Depth: 13 km ID:us2010ciay
40˚N
38˚N
36˚N
34˚N
32˚N
100˚W
95˚W
14862 responses in 753 ZIP codes (Max CDI = V)
100 km
INTENSITY
I
II-III
IV
V
VI
VII
VIII
IX
X+
SHAKING
Not felt
Weak
Light
Moderate
Strong
Very strong
Severe
Violent
Extreme
DAMAGE
none
none
none
Very light
Light
Moderate
Moderate/Heavy
Heavy
V. Heavy
Processed: Tue Apr 16 08:12:18 2013
c)
Slaughterville OK
Spectral Acceleration - 1 Hz
1e-072e-075e-071e-062e-065e-061e-052e-055e-051e-042e-045e-041e-03
Acceleration (g)
d)
Slaughterville OK
Spectral Acceleration - 1 Hz
1e-072e-075e-071e-062e-065e-061e-052e-055e-051e-042e-045e-041e-03
Acceleration (g)

Figure 6

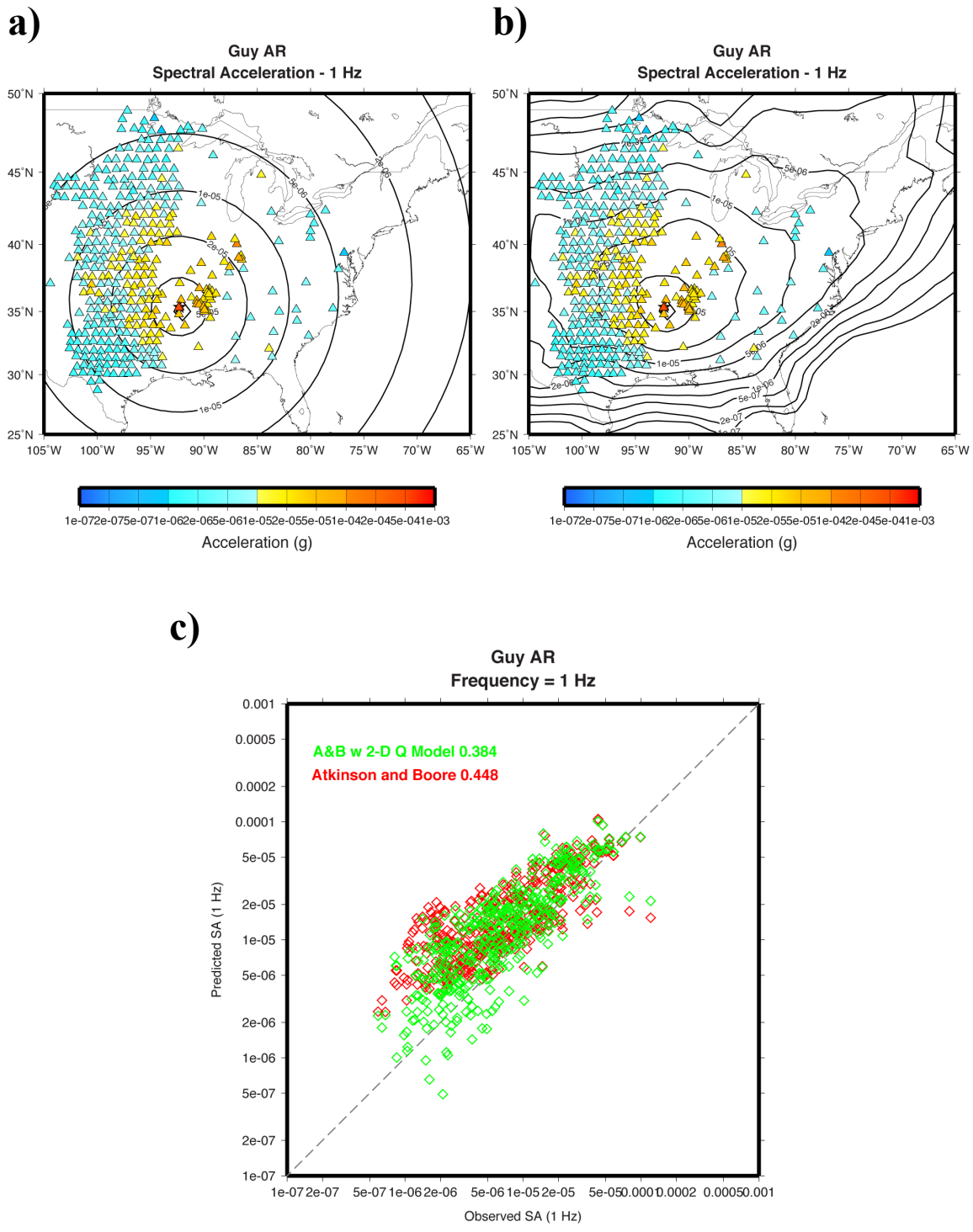
a)
Guy AR
Spectral Acceleration - 1 Hz
b)
Guy AR
Spectral Acceleration - 1 Hz
1e-072e-075e-071e-062e-065e-061e-052e-055e-051e-042e-045e-041e-03
Acceleration (g)
c)
Guy AR
Frequency = 1 Hz
A&B w 2-D Q Model 0.384
Atkinson and Boore 0.448
Predicted SA (1 Hz)
Observed SA (1 Hz)

Figure 7

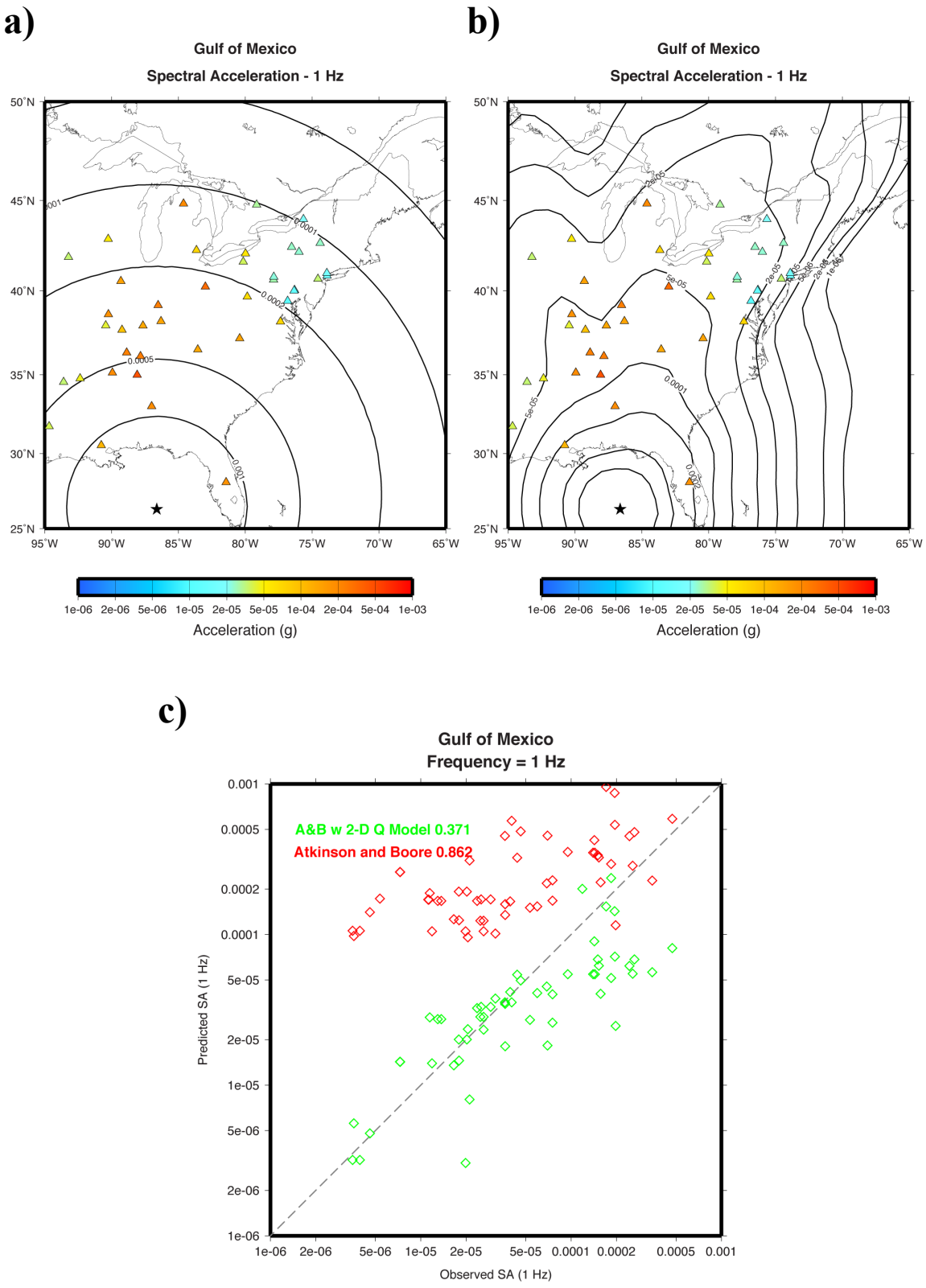
a)
Gulf of Mexico
Spectral Acceleration - 1 Hz
50°N
45°N
40°N
35°N
30°N
25°N
95°W
90°W
85°W
80°W
75°W
70°W
65°W
1e-06 2e-06 5e-06 1e-05 2e-05 5e-05 1e-04 2e-04 5e-04 1e-03
Acceleration (g)
b)
Gulf of Mexico
Spectral Acceleration - 1 Hz
Acceleration (g)
c)
Gulf of Mexico
Frequency = 1 Hz
A&B w 2-D Q Model 0.371
Atkinson and Boore 0.862
Predicted SA (1 Hz)
Observed SA (1 Hz)
0.001
0.0005
0.0002
0.0001
5e-05
2e-05
1e-05
5e-06
2e-06
1e-06

Figure 8

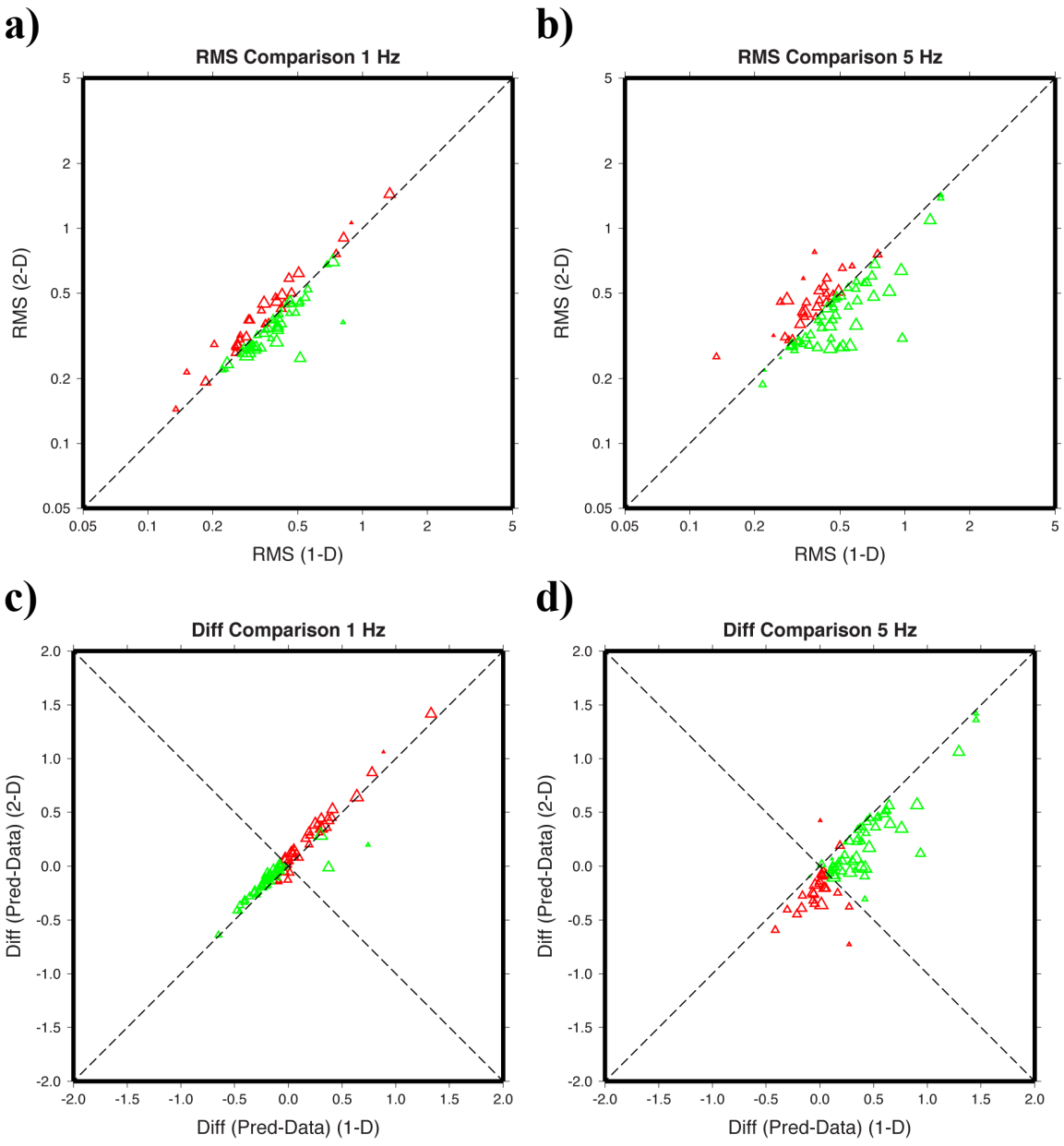
a)
RMS Comparison 1 Hz
RMS (2-D)
RMS (1-D)
b)
RMS Comparison 5 Hz
RMS (2-D)
RMS (1-D)
c)
Diff Comparison 1 Hz
Diff (Pred-Data) (2-D)
Diff (Pred-Data) (1-D)
d)
Diff Comparison 5 Hz
Diff (Pred-Data) (2-D)
Diff (Pred-Data) (1-D)

Figure 9

a)

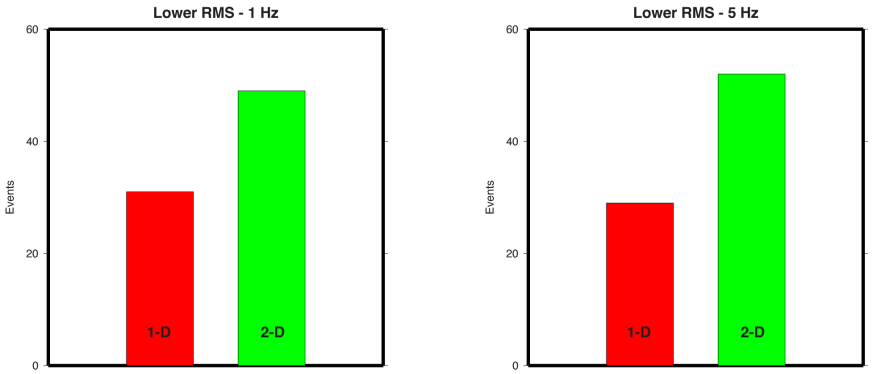

b)

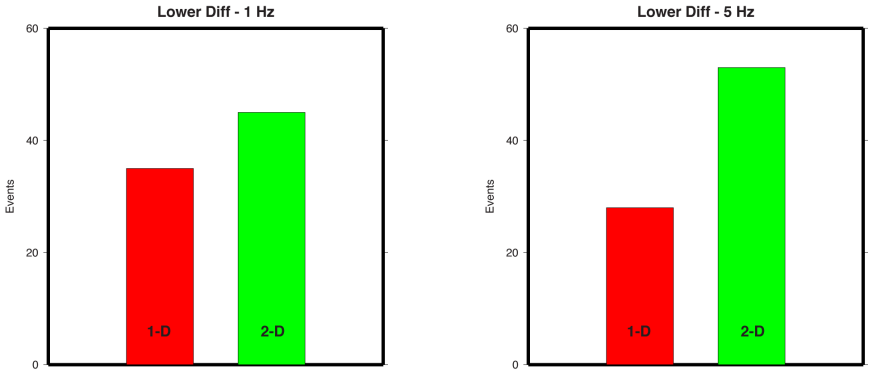

c)

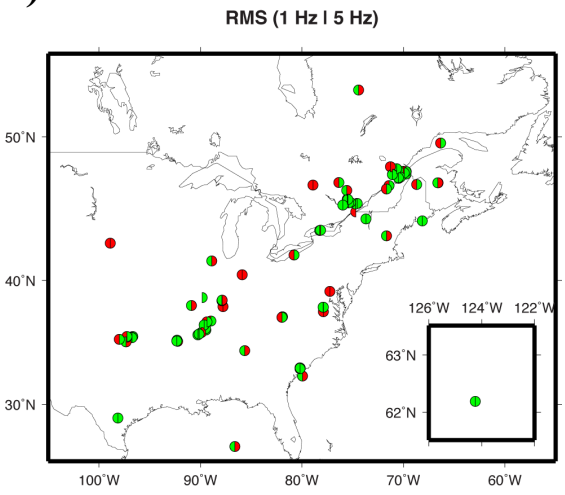

d)

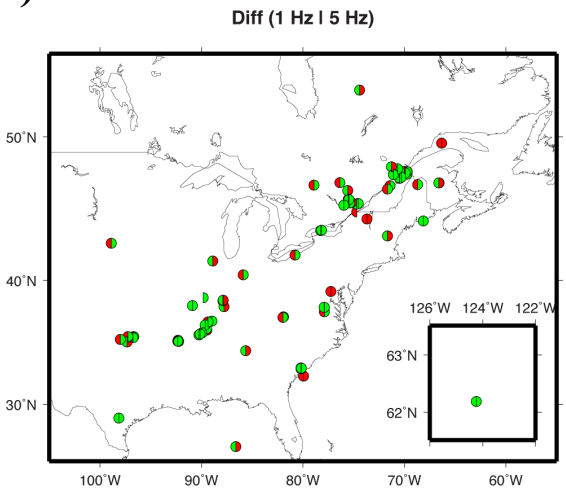

Figure 10

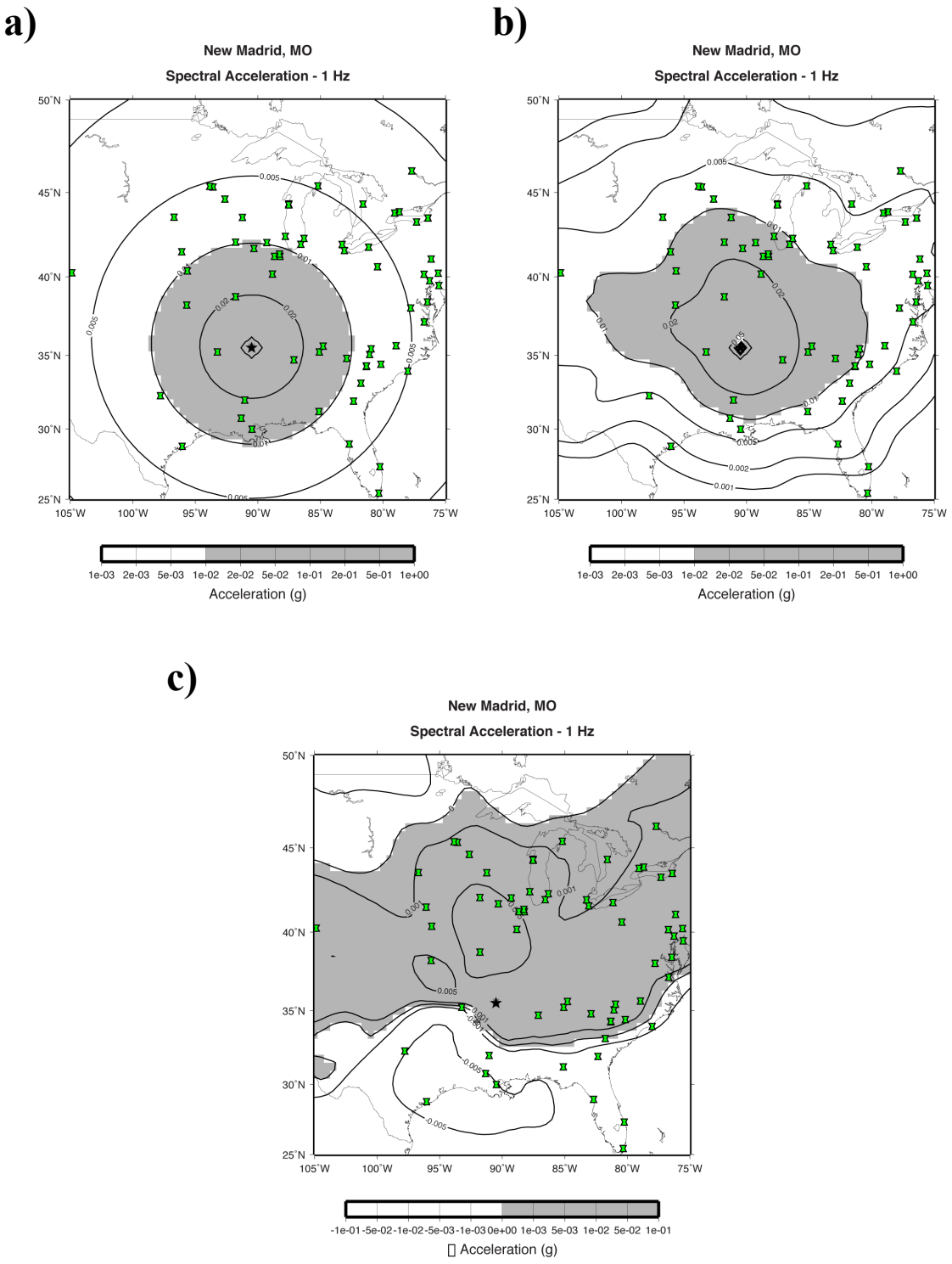
a)
New Madrid, MO
Spectral Acceleration - 1 Hz
50°N
45°N
40°N
35°N
30°N
25°N
105°W
100°W
95°W
90°W
85°W
80°W
75°W
0.005
0.001
0.002
0.02
1e-03 2e-03 5e-03 1e-02 2e-02 5e-02 1e-01 2e-01 5e-01 1e+00
Acceleration (g)
b)
New Madrid, MO
Spectral Acceleration - 1 Hz
0.005
0.001
0.02
0.01
0.002
0.001
1e-03 2e-03 5e-03 1e-02 2e-02 5e-02 1e-01 2e-01 5e-01 1e+00
Acceleration (g)
c)
New Madrid, MO
Spectral Acceleration - 1 Hz
0.001
0.005
0.001
0.005
-1e-01 -5e-02 -1e-02 -5e-03 -1e-03 0e+00 1e-03 5e-03 1e-02 5e-02 1e-01
Acceleration (g)

Figure 11

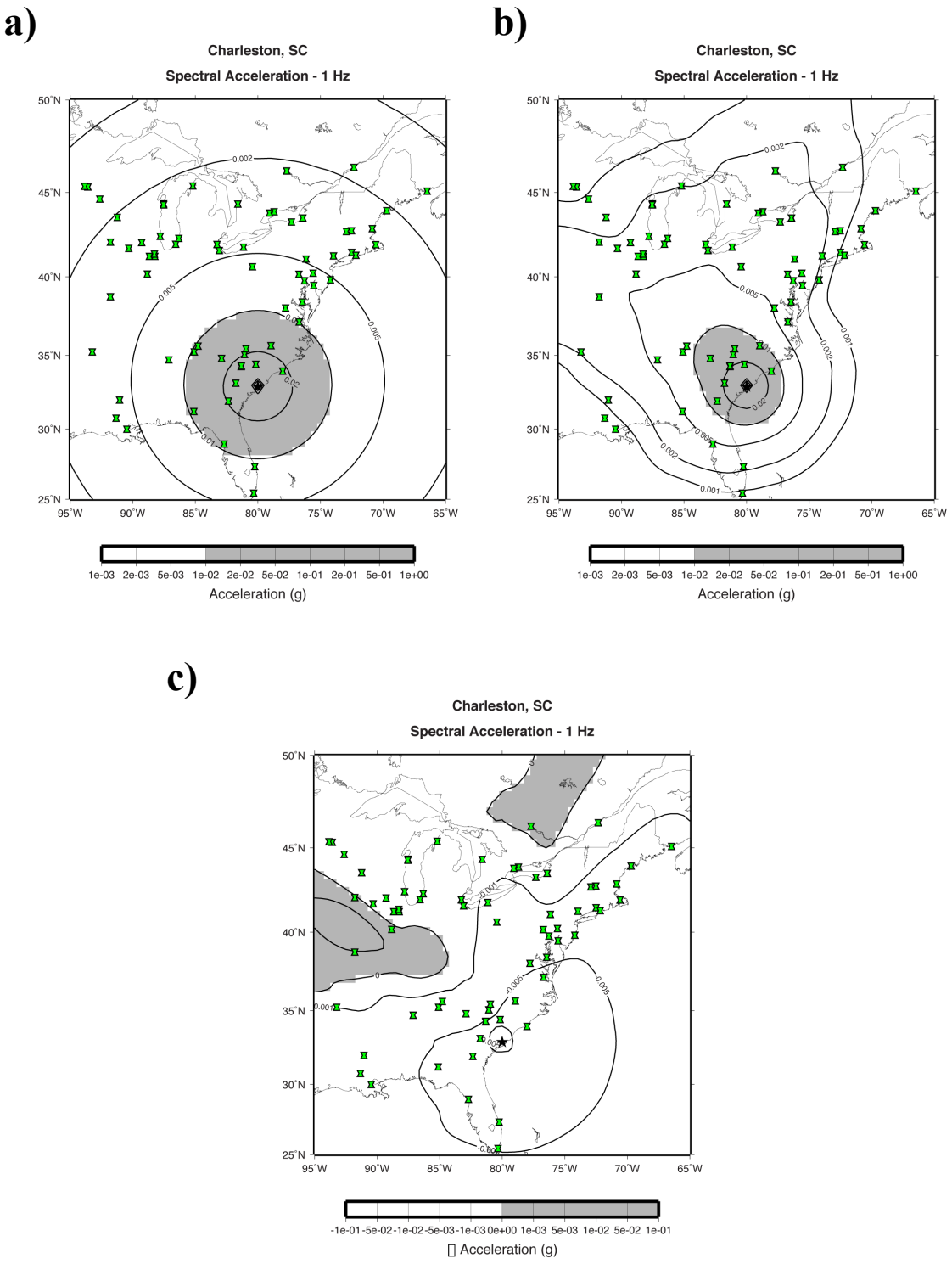
a)
Charleston, SC
Spectral Acceleration - 1 Hz
50°N
45°N
40°N
35°N
30°N
25°N
95°W
90°W
85°W
80°W
75°W
70°W
65°W
0.002
0.005
0.01
0.02
0.001
1e-03 2e-03 5e-03 1e-02 2e-02 5e-02 1e-01 2e-01 5e-01 1e+00
Acceleration (g)
b)
Charleston, SC
Spectral Acceleration - 1 Hz
0.002
0.005
0.001
0.01
0.02
1e-03 2e-03 5e-03 1e-02 2e-02 5e-02 1e-01 2e-01 5e-01 1e+00
Acceleration (g)
c)
Charleston, SC
Spectral Acceleration - 1 Hz
0.001
0.005
-1e-01 -5e-02 -1e-02 -5e-03 -1e-03 0e+00 1e-03 5e-03 1e-02 5e-02 1e-01
Acceleration (g)

Figure 12

a)

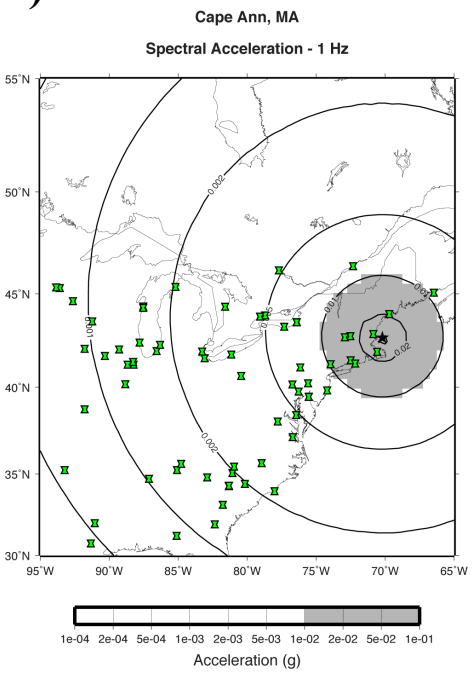

b)

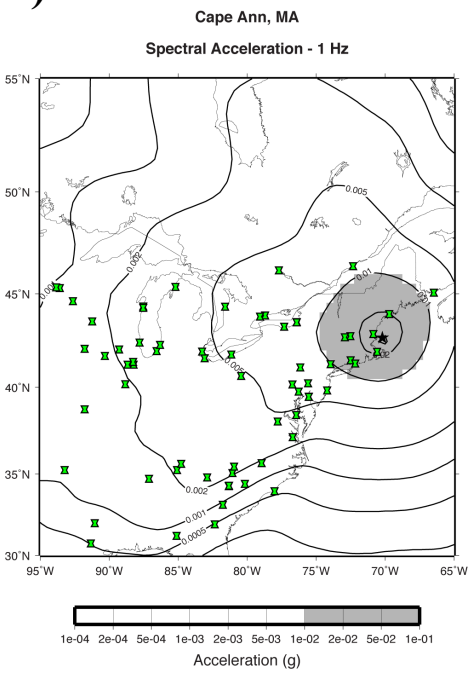

c)